Negative impact of carbapenem methylation on the reactivity of β-lactams for cysteine acylation revealed by quantum calculations and kinetic analyses

Nicholus Bhattacharjee, Sébastien Triboulet, Vincent Dubée, Matthieu Fonvielle, Zainab Edoo, Jean-Emmanuel Hugonnet, Mélanie Etheve-Quelquejeu, Jean-Pierre Simorre, Martin J. Field, Michel Arthur, et al.

AMERICAN SOCIETY FOR MICROBIOLOGY | Antimicrobial Agents and Chemotherapy®

CHEMISTRY; BIOSYNTHESIS

Negative Impact of Carbapenem Methylation on the Reactivity of β-Lactams for Cysteine Acylation as Revealed by Quantum Calculations and Kinetic Analyses

Nicholus Bhattacharjee,[a] Sébastien Triboulet,[b] Vincent Dubée,[b] Matthieu Fonvielle,[b] Zainab Edoo,[b] Jean-Emmanuel Hugonnet,[b] Mélanie Ethève-Quelquejeu,[c] Jean-Pierre Simorre,[a,d] Martin J. Field,[d,e] Michel Arthur,[b] Catherine M. Bougault[a]

[a]Université Grenoble Alpes, CNRS, CEA, IBS, Grenoble, France
[b]Sorbonne Université, Sorbonne Paris Cité, Université Paris Descartes, Université Paris Diderot, INSERM, Centre de Recherche des Cordeliers, CRC, Paris, France
[c]Université Paris Descartes, CNRS UMR 8601, Paris, France
[d]Université Grenoble Alpes, CNRS, CEA, BIG, LCBM (UMR 5249), Grenoble, France
[e]ILL Theory Group, ILL, Grenoble, France

ABSTRACT The *Enterococcus faecium* L,D-transpeptidase (Ldt_{fm}) mediates resistance to most β-lactam antibiotics in this bacterium by replacing classical peptidoglycan polymerases. The catalytic Cys of Ldt_{fm} is rapidly acylated by β-lactams belonging to the carbapenem class but not by penams or cephems. We previously reported quantum calculations and kinetic analyses for Ldt_{fm} and showed that the inactivation profile is not determined by differences in drug binding (K_D [equilibrium dissociation constant] values in the 50 to 80 mM range). In this study, we analyzed the reaction of a Cys sulfhydryl with various β-lactams in the absence of the enzyme environment in order to compare the intrinsic reactivity of drugs belonging to the penam, cephem, and carbapenem classes. For this purpose, we synthesized cyclic Cys-Asn (cCys-Asn) to generate a soluble molecule with a sulfhydryl closely mimicking a cysteine in a polypeptide chain, thereby avoiding free reactive amino and carboxyl groups. Computational studies identified a thermodynamically favored pathway involving a concerted rupture of the β-lactam amide bond and formation of an amine anion. Energy barriers indicated that the drug reactivity was the highest for nonmethylated carbapenems, intermediate for methylated carbapenems and cephems, and the lowest for penams. Electron-withdrawing groups were key reactivity determinants by enabling delocalization of the negative charge of the amine anion. Acylation rates of cCys-Asn determined by spectrophotometry revealed the same order in the reactivity of β-lactams. We concluded that the rate of Ldt_{fm} acylation is largely determined by the β-lactam reactivity with one exception, as the enzyme catalytic pocket fully compensated for the detrimental effect of carbapenem methylation.

KEYWORDS β-lactam, DFT mechanistic investigations, L,D-transpeptidase, concerted β-lactam ring opening, cysteine acylation

L,D-Transpeptidases (Ldts) play a major role in peptidoglycan synthesis only in a few pathogenic bacteria, including *Mycobacterium tuberculosis*, *Mycobacterium abscessus*, and *Clostridium difficile* (1). In other bacteria, the peptidoglycan is mainly or exclusively cross-linked by D,D-transpeptidases, commonly referred to as penicillin-binding proteins (PBPs) (2). Ldts and PBPs differ by the catalytic nucleophile (Cys versus Ser) (1). Ldts and PBPs also differ by their inactivation profiles, as Ldts are effectively inactivated only by carbapenems and some cephems, whereas PBPs are potentially inactivated by all β-lactam classes (Fig. 1) (3). The efficacy of the active-site cysteine acylation of the

Citation Bhattacharjee N, Triboulet S, Dubée V, Fonvielle M, Edoo Z, Hugonnet J-E, Ethève-Quelquejeu M, Simorre J-P, Field MJ, Arthur M, Bougault CM. 2019. Negative impact of carbapenem methylation on the reactivity of β-lactams for cysteine acylation as revealed by quantum calculations and kinetic analyses. Antimicrob Agents Chemother 63:e02039-18. https://doi.org/10.1128/AAC.02039-18.

Address correspondence to Michel Arthur, michel.arthur@crc.jussieu.fr, or Catherine M. Bougault, catherine.bougault@ibs.fr.

N.B. and S.T. contributed equally to this work as first authors; M.A. and C.M.B. contributed equally to this work as principal investigators.

Received 21 September 2018
Returned for modification 26 October 2018
Accepted 29 January 2019
Accepted manuscript posted online 4 February 2019
Published 27 March 2019

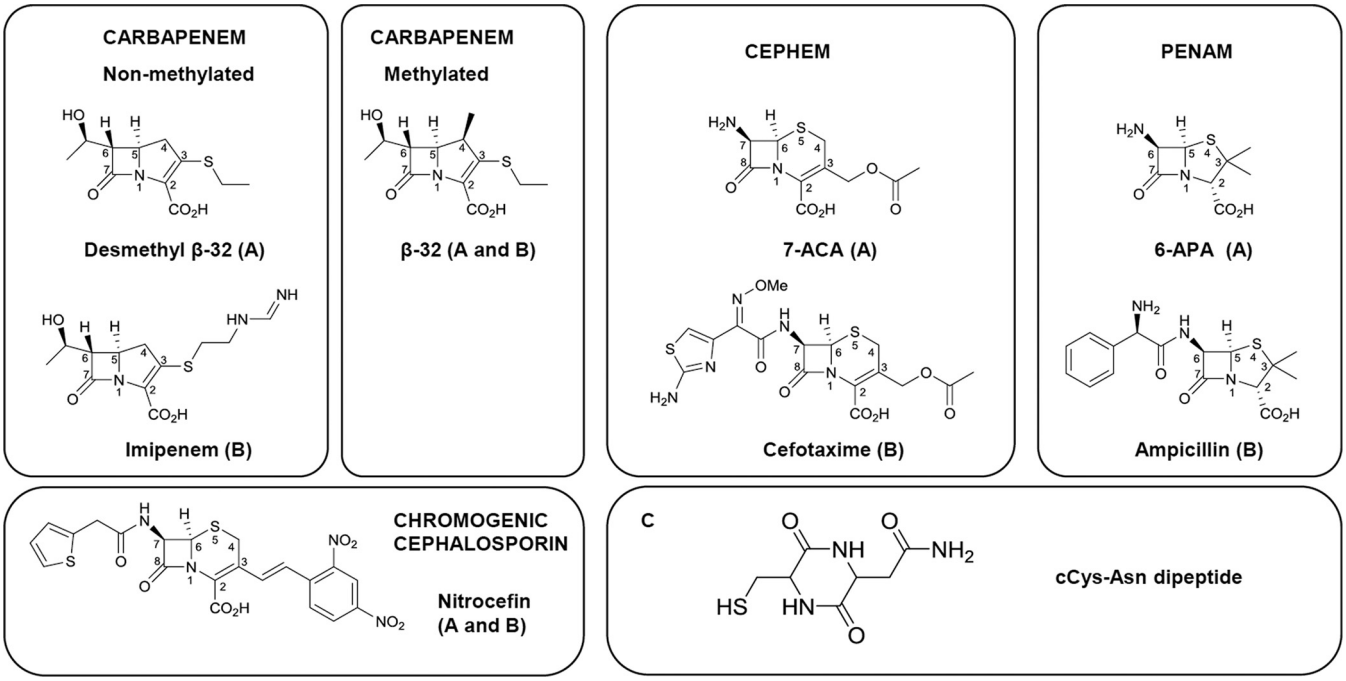

FIG 1 Structures of the cCys-Asn cyclic dipeptide and of the β-lactams used in this study. (A and B) β-Lactams used for theoretical calculations and kinetic analyses, respectively. Different drugs were used for these two approaches, as small molecules (e.g., 6-APA and 7-ACA) were chosen to limit computational time but were not suitable for kinetic analyses due to lack of sensitivity in the spectrophotometric assay.

Enterococcus faecium Ldt (Ldt_{fm}) by β-lactams was previously reported to be 150-fold higher for the carbapenem imipenem than for the cephem ceftriaxone and 840-fold higher for imipenem than for the penam ampicillin (4). Ineffective acylation of Ldt_{fm} by ampicillin coupled to acyl enzyme instability results in the total absence of antibacterial activity (4).

Exploring the basis for the inactivation profile of Ldt_{fm} revealed that variations in the side chains of the β-lactams are not key specificity determinants for several reasons. First, determination of the nuclear magnetic resonance (NMR) structure of the catalytic domain of Ldt_{fm} acylated by ertapenem indicated that the side chain of the β-lactam is not stabilized by any protein-drug interaction (5). Second, comparison of carbapenems with different side chains revealed only minor differences in the acylation efficacy (6). The same observation was made for cephems and penams (4), with, in the former case, the noticeable exception of nitrocefin, which acylates Ldt_{fm} more rapidly than imipenem, due to the unusual electron-withdrawing property of its side chain (7). Third, the affinity of a catalytically inactive form of Ldt_{fm}, obtained by replacing the catalytic Cys with Ala, revealed no significant difference in the K_D (equilibrium dissociation constant) values for representatives of the carbapenems (ertapenem), cephems (ceftriaxone), and penams (ampicillin), i.e., 50, 44, and 79 mM, respectively (4). The last observation also suggested that the inactivation profile is determined by the chemical step of the reaction rather than by the affinity of the enzyme for the β-lactams (4). This prompted us to investigate in this paper the intrinsic reactivity of β-lactams for cysteine by two approaches. First, quantum calculations were performed to identify thermodynamically favored paths for the acylation reaction involving representatives of the three β-lactam classes. This provided access to a comparison of the energy barrier for the various drugs. For these calculations, the sulfhydryl was incorporated into a cyclic dipeptide, cCys-Asn, to mimic as closely as possible a cysteine in a polypeptide chain and to avoid undesired intramolecular interactions. In the second approach, we synthesized the dipeptide cCys-Asn and determined by spectrophotometry the kinetics of its acylation by β-lactams. We also compared apparent second-order rate constants for acylation of Ldt_{fm} and of cCys-Asn by the β-lactams. The latter approach provided

insight into the increase of the acylation rate due to the catalytic properties of the enzyme.

RESULTS AND DISCUSSION

Computation of reaction paths for the acylation of cCys-Asn by β-lactams. The cCys-Asn dipeptide was docked with each of the β-lactams using the pDynamo molecular modeling library (8) with the semiempirical AM1 potential (9) while constraining the distance between the dipeptide sulfur and the β-lactam carbonyl carbon atoms to 2.5 Å. Two relative orientations of the dipeptide and the β-lactam were initially considered to simulate a syn- or anti-periplanar attack by the dipeptide sulfur with respect to the β-lactam nitrogen lone pair. Initial calculations of (2*S*,5*R*,6*R*)-6-amino-3,3-dimethyl-7-oxo-4-thia-1-azabicyclo[3.2.0]heptane-2-carboxylic acid (6-APA), 3-(acetyloxymethyl)-7-amino-8-oxo-5-thia-1-azabicyclo[4.2.0]oct-2-ene-2-carboxylic acid (7-ACA), or (4*R*,5*R*,6*S*)-6[(1*R*)-1-hydroxyethyl]-3-ethylsulfanyl-4-methyl-7-oxo-1-azabicyclo [3.2.0]hept-2-ene-2-carboxylic acid (β-32) attacks by small nucleophiles, such as hydroxide and methanethiolate, showed that the syn-periplanar attack is energetically favored in all cases due to the steric hindrance effect imposed by the fused ring (see Fig. S1 in the supplemental material). This conclusion is consistent with previous studies on the hydrolysis, methanolysis, or thiolysis of penams (10, 11) and on the hydrolysis of cephems (12) and carbapenems (13). Thus, noncovalent β-lactam:cCys-Asn complexes were generated in a syn-periplanar configuration and their geometry was further optimized at the density functional theory (DFT) level within ORCA using the B3LYP hybrid or the BP86 GGA functionals together with the Ahlrichs triple-zeta valence plus polarization basis set (see Materials and Methods for further details). The structures of these prereacting complexes obtained with the B3LYP functional are depicted in Fig. S2.

To generate the reaction paths, possible hypothetical intermediate structures were constructed and optimized from the initial structures of the noncovalent β-lactam:cCys-Asn complexes through consecutive steps involving (i) the deprotonation of cCys-Asn sulfhydryl, (ii) the attack of the β-lactam carbonyl carbon, and, in different relative orders, (iii and iv) the opening of the β-lactam ring and the protonation of its nitrogen. The reactant, intermediate, and product structures were then assembled into complete or partial putative pathways, which were refined using the nudged elastic band (NEB) reaction path-finding algorithm implemented in the pDynamo library (14, 15). Further details about the procedure and its limitations and difficulties are given in Materials and Methods.

Geometry-optimized structures of the β-lactam:cCys-Asn noncovalent complexes. 6-APA, 7-ACA, desmethyl-β-32, and β-32 were docked on cCys-Asn and the geometry of the noncovalent complex was optimized using DFT calculations. These structures superimposed with the published X-ray structures of 6-APA, cephaloglycin, imipenem, and meropenem with root mean square deviations (RMSD) of 0.076, 0.265, 0.109, and 0.171 Å, respectively, on the common heavy atoms (Cambridge database accession codes AMPENA01, CEPGLY, SAHSOJ, and VUCJEI for 6-APA, cephaloglycin, imipenem, and meropenem, respectively). The stability of the conformation of the five- and six-membered rings adjacent to the β-lactam ring in 6-APA and 7-ACA, respectively, was investigated in the noncovalent complex (Fig. S3). The S4-down conformation was preferred by 0.9 kcal mol^{-1} over the S4-up conformation for 6-APA. 7-ACA displayed the opposite preference (S5-up more stable by 2.9 kcal mol^{-1}). These values are consistent with published results obtained on model penams (16) and cephems (17). As the interconversion of the β-lactam-adjacent rings of 6-APA and 7-ACA is expected to occur with low energy barriers, the two conformations were considered in further studies. Of note, all β-lactam:cCys-Asn noncovalent complexes are stabilized by a hydrogen-bond interaction between the amide proton of the Asn side chain and the β-lactam carboxylate (Fig. S2).

Identification of possible intermediates in the acylation of cCys-Asn by β-lactams. Possible intermediates were previously considered for hybrid potential

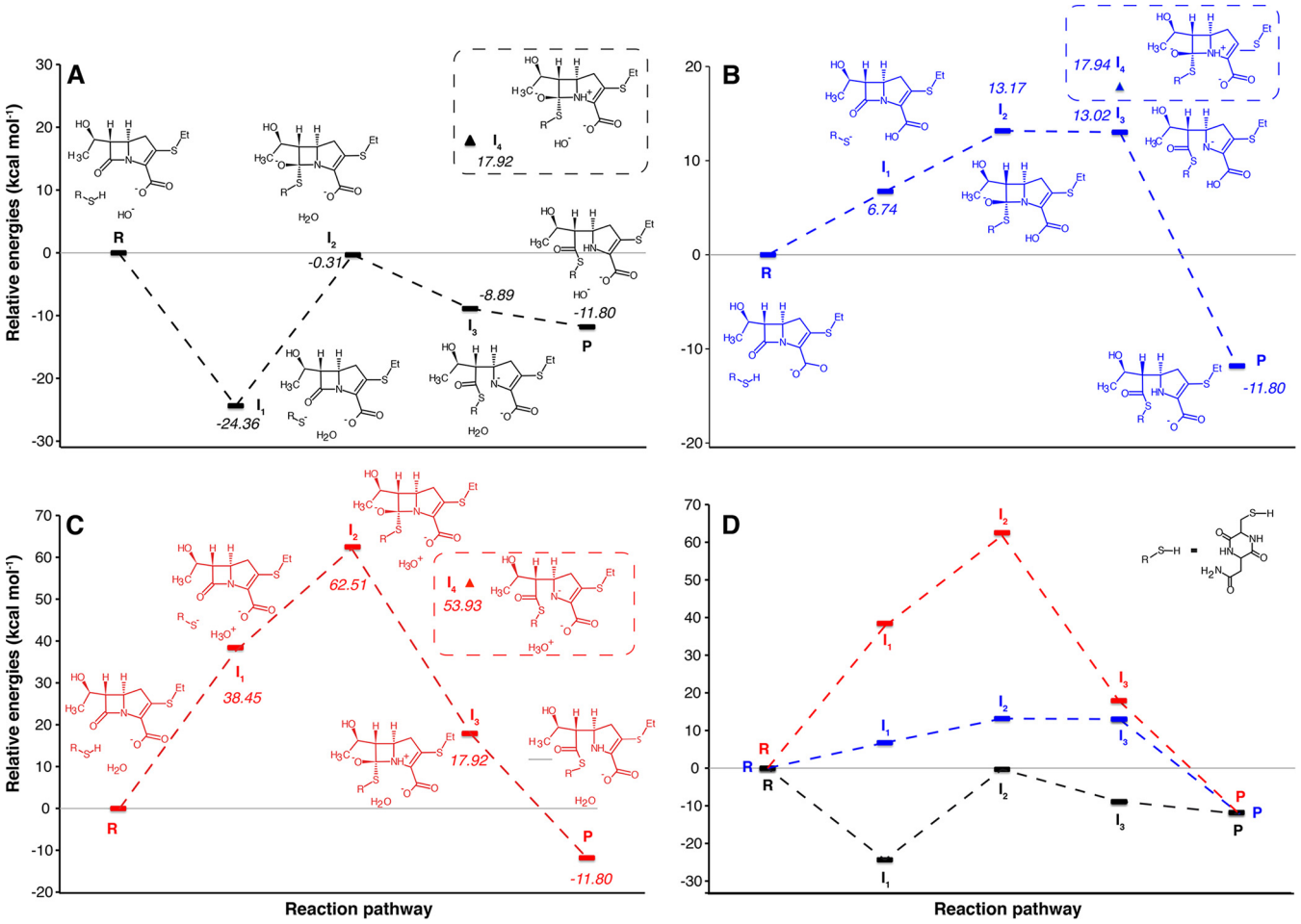

FIG 2 Alternative pathways considered for the acylation of the cyclodipeptide cCys-Asn by the nonmethylated carbapenem desmethyl-β-32. The energy profiles and the structures of intermediates are shown for three pathways initiated by the transfer of the sulfhydryl proton of Cys to OH^- from the solvent (A), to the β-lactam carboxylate (B), or to H_2O from the solvent (C). The remaining panel (D) shows the superimposition of the energy profiles appearing in panels A, B, and C. Intermediates that were disregarded because of their high energy are circled with dashed lines. R, reactants; P, products; I, intermediates; R-SH, cyclodipeptide cCys-Asn.

simulation of the acylation of *E. faecium* L,D-transpeptidase (Ldt_{fm}) by the carbapenem ertapenem (18). In this study, we systematically investigated the energetics of the different acylation paths for cCys-Asn and the representatives of the three β-lactam classes (Fig. 1) by considering the four steps detailed in Fig. 2 for desmethyl-β-32, namely, (i) the cCys-Asn sulfhydryl deprotonation, (ii) the nucleophilic attack of the β-lactam ring, and (iii and iv) the opening of the β-lactam ring followed or preceded by the protonation of its nitrogen. The energies of the corresponding hypothetical intermediates were systematically determined using the B3LYP hybrid and BP86 GGA functionals. Since the two methods provided similar results, as exemplified by the analysis of 6-APA in Fig. S4, only the B3LYP results are presented below.

For the first step, the cysteinyl dipeptide is introduced as a thiol. It is well documented, and our calculations confirm, that thiolate is, however, a stronger nucleophile. A proton transfer from the cysteine to an appropriate acceptor is thus necessary. We considered hydroxide from solvent (Fig. 2A), the β-lactam carboxylate (Fig. 2B), and water (Fig. 2C) as potential proton acceptors. For all β-lactams, proton transfer from the dipeptide sulfhydryl to a hydroxide from the solvent was exothermic, whereas the other two alternative proton transfers were endothermic (data are shown for desmethyl-β-32 in Fig. 2). The former path is fully discussed here since it led to overall lower-energy intermediates (Table 1). However, we could not completely disregard proton transfer to the β-lactam carboxylate since this path involved lower energy barriers in the subse-

TABLE 1 B3LYP relative energies of intermediates and transition states with respect to the noncovalent β-lactam:cCys-Asn complex for penams, cephems, and carbapenems after initial proton transfer from the cCys-Asn sulfhydryl to a solvent hydroxide

	Energy (kcal mol^{-1})					
		Oxyanion path[a]		Concerted path[a]		
β-Lactam	Intermediate I_1 after proton transfer	Oxyanion intermediate I_2	I_2-to-I_3 oxyanion transition-state	β-lactam:cCys-Asn intermediate I_3	I_1-to-I_3 concerted transition-state (TS_{13})	Final adduct P after N-1 protonation
Desmethyl-β-32	−24.36	−0.31	8.83	−8.89	−7.92	−11.80
β-32	−23.29	1.23	13.27	−6.13	−2.17	−8.58
7-ACA S5-up	−21.75	1.68	ND[e]	−6.13	−2.18	−24.36[b]
7-ACA S5-down	−22.37	5.51	6.05	−3.06	−2.10	−26.50[b]
6-APA S4-up	−24.05	1.38	20.20	−9.80[c]	4.99	0.15
6-APA S4-down	−22.67	2.76	ND[e]	−4.90[c]	2.08	−6.89
Nitrocefin	−22.67	−3.06	NA[f]	−28.95	−11.66	−6.59[d]

[a]The oxyanion intermediate I_2 is depicted in Fig. 2A for desmethyl-β-32; β-lactam:cCys-Asn intermediates I_3 that result from a concerted attack by the cysteine thiolate and β-lactam ring opening are depicted in Fig. 3 for desmethyl-β-32, β-32, 7-ACA, 6-APA, and nitrocefin.
[b]Formation of the final adduct proceeds not through protonation of N-1 but through elimination of the acetate group.
[c]The negative charge on N-1 delocalized to the sulfur of the adjacent thiazolidine fused ring and led to a more stable intermediate in which the C-5–S-4 bond is cleaved.
[d]The DFT calculation did not converge.
[e]ND, not determined.
[f]NA, not applicable, as N-1 in the nitrocefin product is not protonated due to the delocalization of the negative charge to the dinitrobenzene.

quent attack of the β-lactam ring by the thiolate. The corresponding results are presented in Fig. S5 and Tables S1 and S6 to S9.

For the second step, we considered that the attack of the β-lactam carbonyl by the cysteine thiolate might lead to an oxyanion intermediate (classical addition-elimination mechanism) or to a simultaneous ring opening via a concerted mechanism. The oxyanion intermediate and the subsequent transition state, which leads to ring opening, were both high in energy, as shown for carbapenem desmethyl-β-32 in Fig. 2. This conclusion applies to all β-lactams in the pathways starting either (i) with an initial proton transfer to the solvent hydroxide (Table 1) or (ii) with an initial proton transfer to the β-lactam carboxylate (Table S1). Thus, we investigated a concerted mechanism for the β-lactam ring opening using the nudge elastic band (NEB) approach. A transition state of lower energy than that of the oxyanion was found for all β-lactams (Fig. 3 and Table 1). Thus, formation of the oxyanion could be excluded on energetic criteria.

For the third and fourth steps, we considered that the protonation of the N-1 nitrogen atom of the β-lactam ring might occur before or after ring opening. The protonated carboxylate of the β-lactam ring or the solvent were regarded as potential proton donors, depending upon the intermediates created in the first step. Protonation of N-1 prior to the ring opening was energetically costly (intermediate I_4 in Fig. 2A and B). In comparison, a significant energetic gain is associated with rupture of the β-lactam ring and formation of an amine anion prior to the final protonation step. This may be accounted for by the fact that the negative charge on N-1 is stabilized by resonance with the β-lactam-adjacent ring (carbapenem and cephem) or by the β-lactam-adjacent ring opening (penam).

A methyl substituent in the five-membered ring of carbapenem increases the energy of the transition state. The formation of the thiolate and the subsequent nucleophilic attack of the β-lactam ring proceed through energetically comparable intermediates for the nonmethylated and methylated carbapenems (desmethyl-β-32 versus β-32 [Fig. 3A and B]). In contrast, the transition state obtained for the concerted mechanism was unexpectedly stabilized by almost 6 kcal mol^{-1} in the absence of the methyl group. Comparison of the geometries of the I_1 intermediates preceding the nucleophilic attack indicated that the Δ^2-pyrroline ring is slightly more puckered in desmethyl-β-32 than in β-32 (C-4–C-5–C-6 angle of 122.74° versus 124.66° and C-6–C-7–N-1–C-2 dihedral angle of 123.09° versus 124.97°, respectively) (Table S2). Variations of these angles between the I_1 intermediate and the TS_{13} transition state suggest that the puckering release is greater in the absence of methyl substituent on the

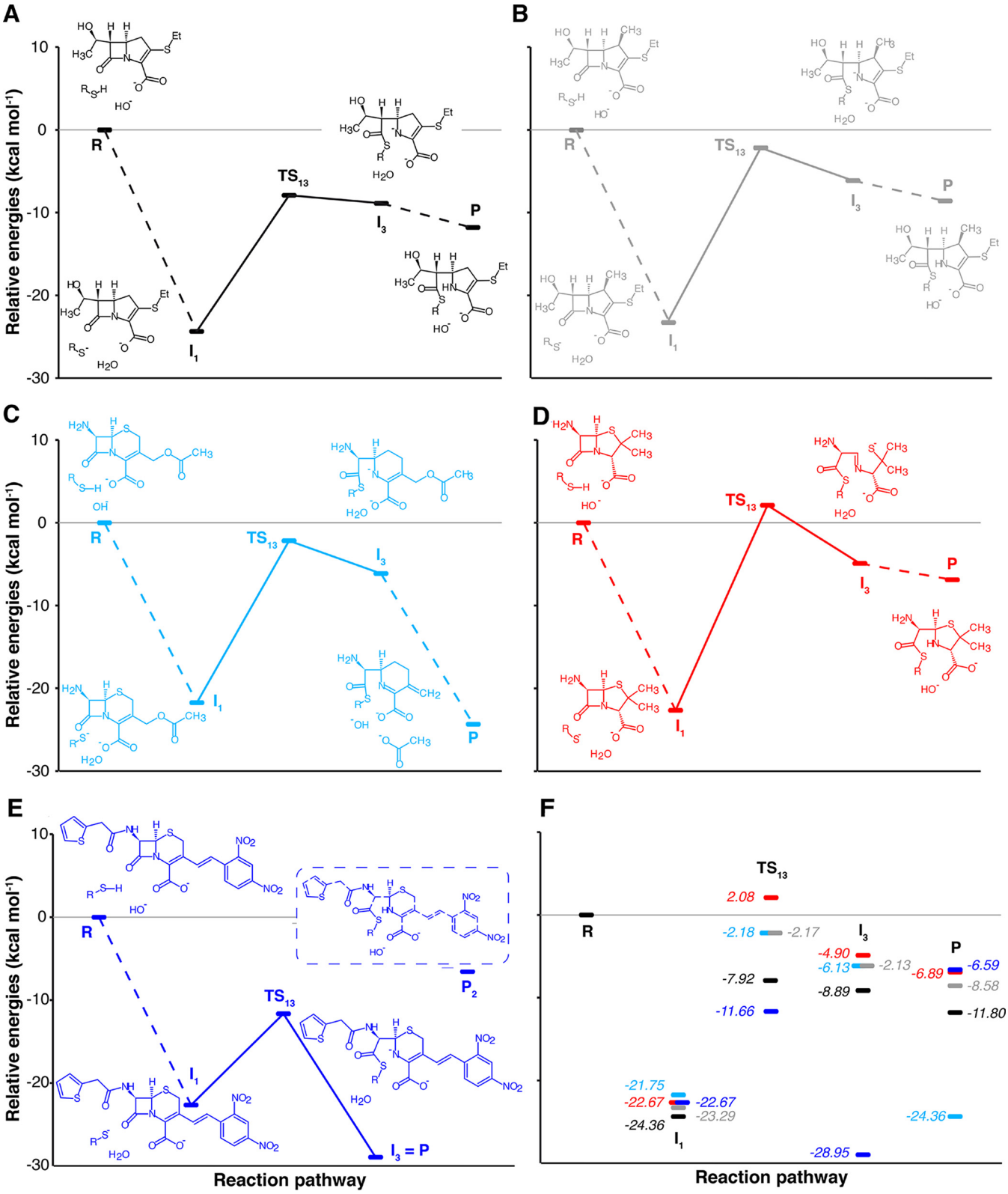

FIG 3 Reaction pathways for the acylation of the cyclodipeptide cCys-Asn by β-lactams. The most favorable pathways are depicted for acylation of cCys-Asn by the nonmethylated carbapenem desmethyl-β-32 (A), the methylated carbapenem β-32 (B), the cephem 7-ACA (C), the penam 6-APA (D), and the chromogenic cephalosporin nitrocefin (E). The most favorable pathways are initiated by the transfer of the sulfhydryl proton of Cys to OH^- from the solvent for the five β-lactams. The remaining panel (F) shows the superimposition of the energy profiles appearing in panels A to E. States that were disregarded because of their high energy are circled with dashed lines. TS, transition states. Solid lines indicate energy barriers involving TSs. Dotted lines indicate energy differences between reactants, intermediates, and products.

TABLE 2 Acylation parameters determined by molecular modeling and kinetic analyses

	Energy barrier (kcal mol^{-1})		Acylation constant (M^{-1} min^{-1})		
β-Lactam class	**β-Lactam**	**Energy**	**β-Lactam**	**cCys-Asn**	**Ldt$_{fm}$[d]**
Carbapenem (non-Me[a])	Desmethyl-β-32	16.4	Imipenem	5.8 ± 0.2	(4.4 ± 0.1) × 10^5
Carbapenem (Me[b])	β-32	21.1	β-32	<0.2	(7.6 ± 0.1) × 10^5
Cephem	7-ACA	19.6	Cefotaxime	<0.2	2,700 ± 100
Penam	6-APA	24.8	Ampicillin	NA[c]	520 ± 20
Chromogenic cephalosporin	Nitrocefin	11.0	Nitrocefin	4.8 ± 0.5	(1.4 ± 0.1) × 10^6

[a]non-Me, nonmethylated.
[b]Me, methylated.
[c]NA, not applicable.
[d]Data are from Triboulet et al. (4) for imipenem and ampicillin, from Edoo et al. (7) for nitrocefin, and from this work for β-32 and cefotaxime.

pyrroline ring (122.74° to 112.79° versus 124.66° to 117.44° for desmethyl-β-32 and β-32, respectively). This may account for the difference in the energy barriers.

Impact of the β-lactam-adjacent ring on the reactivity of carbapenems, cephems, and penams. Our next objective was to specifically compare the possibilities of delocalization of the electron density on N-1 in the three classes of β-lactams. This delocalization is predicted to make the carbonyl carbon of the β-lactam more susceptible to nucleophilic attack and to stabilize the potential amine anion intermediate after the β-lactam ring opening. For carbapenems (Fig. 3A and B), the double bond at the C-2–C-3 position in the Δ^2-pyrroline ring provided the possibility of an allylic rearrangement of the negative charge developing on N-1 (N-1–C-2 double bond formation and protonation of C-3). For the 7-ACA cephem, the negative charge developing on N-1 delocalized to C-2 through a mesomeric effect (Table S3), leading to the departure of the acetate group of the dihydrothiazine ring adjacent to the β-lactam ring (Fig. 3C). This was associated with an 18.23-kcal mol^{-1} energetic gain (Table 1) for the S5-up conformation of the dihydrothiazine that proved to yield the lowest energy barrier for the β-lactam ring opening compared to the S5-down conformation despite the lower stability of the I_1 intermediate and the P product (Table 1). Of note, the energetic barriers for the opening of the β-lactam ring are similar for β-32 and 7-ACA (21.1 and 19.6 kcal mol^{-1}, respectively [Table 2]). For 6-APA, rupture of the C-7–N-1 bond was associated with the opening of the β-lactam-adjacent ring and the negative charge was transferred to its sulfur atom (Fig. 3D and Table S4). Despite the >20-kcal mol^{-1} gain in stabilization of the intermediate obtained by this concerted process, 6-APA yielded the highest energy barrier (24.8 kcal mol^{-1} for the more stable S4-down conformation of the thiazolidine ring [Table 1]). This may be accounted for by the difficulty of delocalizing the negative charge developing on N-1 to the β-lactam-adjacent ring that is saturated in penams. The energy profiles thus predict the following order for the reactivity of β-lactams: nonmethylated carbapenems > methylated carbapenems ≈ cephems > penams (Fig. 3). For the β-lactams with an unsaturated adjacent ring, the length of the N-1–C-2 bond, reflecting its partial double-bond character, at different stages of the reaction pathways is in agreement with the above analysis (Tables S2 and S3). Structures of the TS_{13} transition states for each β-lactam according to the proposed concerted thiolate nucleophilic attack and β-lactam ring opening are depicted in Fig. 4.

Impact of a strong electron-withdrawing group in the side chain of nitrocefin. Chromogenic cephalosporins belonging to the cephem class, such as nitrocefin, have been developed to detect production of β-lactamases and to study their inhibition. The side chain of nitrocefin differs from that of cephems used as antibiotics by the presence of a conjugated system connecting its N-1 to a dinitrophenyl chromogenic ring. Thus, there is no leaving group in nitrocefin and the dinitrophenyl acts as a strong electron-withdrawing group, offering the possibility to test an additional type of β-lactam. The energy profile for acylation of cCys-Asn by nitrocefin (Fig. 3E) revealed that nitrocefin alone or in complex with the cCys-Asn dipeptide is stabilized in the S5-up conformation. The puckering of the β-lactam-adjacent ring diminished as the β-lactam ring opened, since the C-6–N-1–C-2–C-3 dihedral angle decreased from 5.05° in the non-

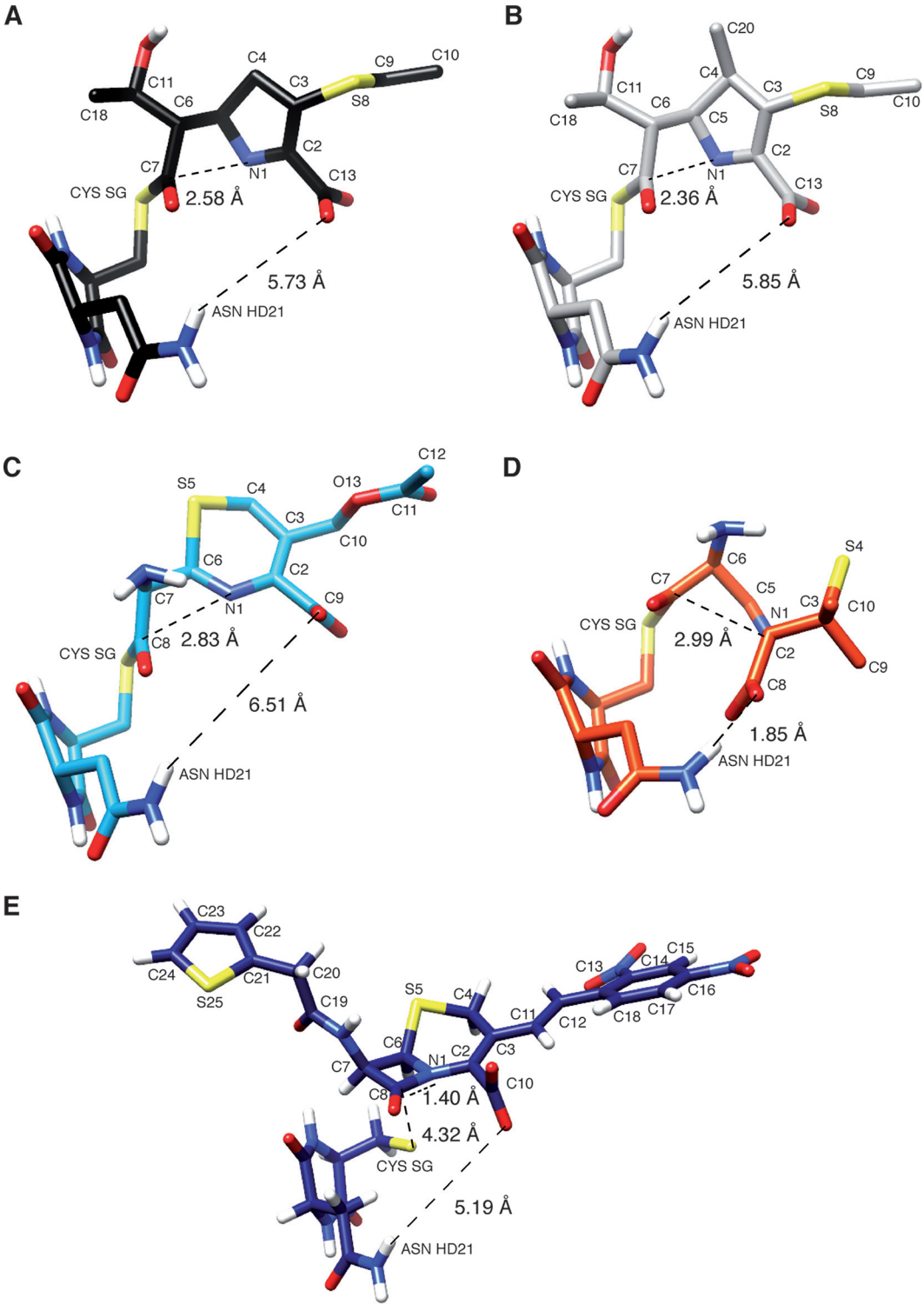

FIG 4 Structure of transition states in the acylation reaction of cCys-Asn by β-lactams. TS_{13} transition states obtained for a concerted thiolate attack and β-lactam ring opening are depicted for the nonmethylated carbapenem desmethyl-β-32 (A), the methylated carbapenem β-32 (B), the cephem 7-ACA in S5-up conformation (C), the penam 6-APA in S4-down conformation (D), and the chromogenic cephalosporin nitrocefin (E). Most transition states resemble the I_3 intermediates with a short cysteine sulfhydryl-to-carbonyl distance, with the exception of nitrocefin. In all transition states but 6-APA, the hydrogen bond between the Asn amide protons and the β-lactam carboxylate is disrupted.

covalent thiolate complex to 1.43° in the transition state and to 0.61° in the I_3 intermediate with the opened β-lactam ring (Table S5). The energy barrier (11.0 kcal mol^{-1}) for the β-lactam ring opening was much lower than that observed for the 7-ACA cephem (19.6 kcal mol^{-1}, as mentioned above), in agreement with the expected impact of resonance on (i) the susceptibility of the carbon carbonyl to nucleophilic attack by the thiolate of the cCys-Asn dipeptide and (ii) the delocalization of the negative charge that develops on the nitrogen of the β-lactam ring of nitrocefin (Table 1).

Kinetic analysis of the acylation of the cyclic dipeptide cCys-Asn by β-lactams. Preliminary experiments were performed to identify a suitable pH for comparison of acylation rates with various β-lactams, i.e., a pH that is sufficiently high for significant deprotonation of the sulfhydryl group of cCys-Asn for nucleophilic attack of the β-lactam ring and sufficiently low to limit the rate of spontaneous hydrolysis of the β-lactam ring. To find a trade-off, the pK_a of the sulfhydryl group of cCys-Asn was determined by spectrophotometry (9.24 ± 0.01 [Fig. S6]). A pH value of 8.2 was chosen (8.4% deprotonation) since the spontaneous rate of hydrolysis of the β-lactams under these conditions was insignificant, enabling acylation rates as low as 0.02 μM min^{-1} to be determined at concentrations of cCys-Asn and β-lactams of 1,000 μM and 100 μM, respectively (Fig. S7).

Acylation of cCys-Asn was detected for the nonmethylated carbapenem imipenem and the chromogenic cephalosporin nitrocefin, but not for the methylated carbapenem β-32 or the cephem cefotaxime (Table 2 and Fig. S7). DFT calculations (above) revealed the lowest energy barriers for the former two compounds, i.e., the nonmethylated carbapenem (desmethyl-β-32, 16.4 kcal mol^{-1}) and nitrocefin (11.0 kcal mol^{-1}). Thus, the computed energy barrier was predictive of the reactivity of β-lactams in the cyclodipeptide acylation assay.

Kinetic analysis of acylation of Ldt_{fm} by β-lactams. Our next objective was to determine whether the differences in the energy barriers are also predictive of the rate of acylation of the active-site Cys residue of Ldt_{fm}. This approach was also used to determine if, and to what extent, the environment of the catalytic Cys in Ldt_{fm} increases the acylation rate. For the nonmethylated carbapenem imipenem, catalysis by Ldt_{fm} led to an 8×10^4-fold increase in the acylation rate (Table 2). A similar enhancement (3×10^5-fold) was observed for nitrocefin. Ldt_{fm} was slowly acylated by the cefotaxime cephem, which did not acylate cCys-Asn at a detectable level. Thus, the absence of reactivity in the cCys-Asn assay correlated with slow acylation of Ldt_{fm}. In contrast, one of the β-lactams under study, the methylated carbapenem β-32, showed an atypical reactivity with Ldt_{fm} in comparison to the dipeptide. The methylation of the carbapenem reduced the acylation rate with the dipeptide at least 29-fold, from 5.8 ± 0.2 M^{-1} min^{-1} to less than 0.2 M^{-1} min^{-1}, in agreement with a 4.7-kcal mol^{-1} difference in the energy barrier. For acylation of Ldt_{fm}, β-32 was as effective as imipenem, leading to a fold increase exceeding 4×10^6 in the catalyzed reaction rate [$<$0.2 M^{-1} min^{-1} versus (7.6 ± 0.1) × 10^5 M^{-1} min^{-1}]. Thus, the catalytic properties of Ldt_{fm} appear to fully compensate for the detrimental effect of the methyl group on β-lactam reactivity. Comparison of nonmethylated and methylated carbapenems indicates that Ldt_{fm} actually displays substrate specificity since these molecules display very different reactivities in the dipeptide assay but similar efficacies in the Ldt_{fm} acylation reaction.

Conclusion. Classical PBPs contain an active-site Ser residue as the nucleophile instead of a Cys residue in L,D-transpeptidases. The pK_a of an aliphatic hydroxyl is on the order of 16 (value for ethanol) (19), indicating that acylation is unlikely to occur at a significant rate at physiological pH in the absence of a catalyst, and, accordingly, the cyclodipeptide cSer-Asn did not react with any of the β-lactams used in this study (data not shown). Of note, methanolysis of amoxicillin has been reported, but the initial rate was very low (8×10^{-8} M^{-1} min^{-1}) (20). For sulfhydryl, the pK_a is much lower, 9.24 ± 0.01, as determined for the cyclic dipeptide cCys-Asn (Fig. S6). This model nucleophile for the noncatalyzed acylation reacted at a detectable level with two β-lactams, nitrocefin and imipenem (a nonmethylated carbapenem), which were also

determined to be the β-lactams with the lowest energy barrier by quantum calculations (Fig. 3 and Table 2). A higher energy barrier was calculated for the methylated carbapenem β-32, which, accordingly, did not detectably react with cCys-Asn. Release of the puckering in desmethyl-β-32 may account for the difference in the energy barriers between methylated and nonmethylated carbapenems.

Previous analyses (4) have shown that Ldt_{fm} displays a low affinity for β-lactams and an absence of any significant specificity for particular drug classes (K_D values ranging from 44 to 79 mM for binding of representatives of the carbapenem, cephem, and penam classes to Ldt_{fm} $C^{442}A$). Hence, the rate enhancement provided by the Ldt_{fm} catalytic cavity is likely to mainly involve a lowering of the energy barrier of the acylation reaction. Still, the observed rate enhancement (on the order of 10^6 [Table 2]) is relatively modest in comparison to the range of rate enhancements determined for enzyme-catalyzed reactions (from 10^6 to 10^{17}) (21). Accordingly, the reactivity of β-lactams, which is proposed to mainly depend upon the electrophilicity of their β-lactam carbonyl carbon and the presence of electron withdrawing group in their side chain for the delocalization of the negative charge developing on N-1, may remain an important factor accounting for the relative acylation efficacies of Ldt_{fm} by β-lactams (nonmethylated carbapenems ≈ nitrocefin > methylated carbapenems ≈ cephems > penams). In contrast, no clear correlation has been observed between the chemical reactivity of β-lactams of the penam and cephem classes and the acylation efficacy of active Ser enzymes displaying D,D-transpeptidase or β-lactamase activity (22). Optimization of β-lactams for inactivation of L,D-transpeptidases, which have recently found potential applications in the treatment of infections due to mycobacteria (23–25), should therefore focus on improving reactivity while preserving sufficient drug stability, although toxicity issues may arise from acylation of human enzymes. Additional properties, including limited acyl enzyme hydrolysis (4) and the irreversibility of the β-lactam ring opening (7), are also important for antibacterial activity.

MATERIALS AND METHODS

Construction of β-lactams and cyclic dipeptide structures. In this work, we investigated the reactivity of β-lactam antibiotics belonging to three different classes, penam, cephem, and carbapenem (Fig. 1), i.e., (2*S*,5*R*,6*R*)-6-amino-3,3-dimethyl-7-oxo-4-thia-1-azabicyclo[3.2.0]heptane-2-carboxylic acid (6-APA) for the penam class, 3-(acetyloxymethyl)-7-amino-8-oxo-5-thia-1-azabicyclo[4.2.0]oct-2-ene-2-carboxylic acid (7-ACA) for the cephem class, (5*R*,6*S*)-6[(1*R*)-1-hydroxyethyl]-3-ethylsulfanyl-7-oxo-1-azabicyclo[3.2.0]hept-2-ene-2-carboxylic acid (desmethyl-β-32) for nonmethylated carbapenems, and (4*R*,5*R*,6*S*)-6[(1*R*)-1-hydroxyethyl]-3-ethylsulfanyl-4-methyl-7-oxo-1-azabicyclo[3.2.0]hept-2-ene-2-carboxylic acid (β-32) (6) for methylated carbapenems. We also investigated (6*R*,7*R*)-3-[(*E*)-2-(2,4-dinitrophenyl)ethenyl]-8-oxo-7-[(2-thiophen-2-ylacetyl)amino]-5-thia-1-azabicyclo[4.2.0]oct-2-ene-2-carboxylic acid (nitrocefin), which is a chromogenic cephem with an unusual side chain containing a dinitrophenyl group.

Initial three-dimensional structures of 6-APA, 7-ACA, and nitrocefin were generated through the Avogadro software (26) from the EMBL-EBI database references ChEMBL 1236749, 1615585, and 480517, respectively. Initial structures for β-32 and desmethyl-β-32 were derived from the imipenem X-ray structure deposited under the accession code SAHSOJ in the Cambridge database (27). The initial structure of the cyclic dipeptide (3*S*,6*S*)-3-carbamoylmethyl-6-mercaptomethyl-piperazine-2,5-dione (cCys-Asn) was built from the atomic coordinates of the cAsp-Asp dipeptide structure (28) in Avogadro. The obtained structure was run through the NAMD molecular dynamics (MD) simulation (29) with the CHARMM force field within a TIP3P water box for 5 ps, and the 10 energy-minimized structures served as input for density functional theory (DFT) calculations.

Investigation of the reaction paths. The reactions we are studying are complex, involving large, loosely bound species in solvent. Ideally, a full computational study would imply the generation of an ensemble of representative reactive trajectories for each complex using MD simulations and quantum chemical (QC) potentials in explicit solvent. However, this is out of reach with current computational resources. Instead, we performed QC calculations of the reactions with an implicit solvent model and the following strategy. First, we extracted representative starting structures for mechanistic studies from our MD simulations in explicit solvent. These structures, for each β-lactam and cCys-Asn pair (see Tables S10 to S16), were then geometry optimized in implicit solvent at the DFT level. Second, we generated structures for hypothetical reaction intermediates from the initial structures by consecutively (i) deprotonating the cCys-Asn sulfhydryl, (ii) attacking the β-lactam carbonyl carbon, and, in different relative orders (iii and iv), opening the β-lactam ring and protonating its nitrogen. These intermediates were obtained either by construction, followed by geometry optimization, or by using relaxed surface scans in which specific interatomic distances were constrained to force particular configurations. Third, intermediates were assembled piecewise into putative pathways, which were then refined using the

nudged elastic band (NEB) reaction path-finding algorithm implemented in the pDynamo library (14, 15). The latter produces a trajectory of equally spaced structures along an approximate minimum energy path that encompasses reactants, intermediates, and products. Previous work has shown that reasonable approximations to the transition states along the pathway can be obtained by interpolating the highest-energy structures from the trajectories (15).

We would like to emphasize several points about the above-described procedure. First we note that it is not automatic and that many different mechanistic hypotheses had to be explored before obtaining the paths reported in this paper. Even so, it is clear that these paths are not definitive but only representative of the many that are likely possible in solution. Second, the reactions are complex, involving large conformational rearrangements in addition to the chemical steps. This meant that a full path usually had several energy barriers, mostly corresponding to conformational changes, and that the number of structures required to fully resolve the paths was often large (up to 500). Third, we verified the nature of the crucial intermediate and transition state structures using frequency calculations. However, due to the flexibility of the structures, especially before reaction, we often found "irrelevant" modes with imaginary frequencies involving atoms far from the reaction site. Initially, we further refined these structures to remove these modes but found the resulting differences in energy to be minimal. Therefore, we did not do it consistently, as long as, for example, the modes for bond breaking and forming were appropriate. Finally, we also employed other approaches to determine or refine the paths—for example, the conjugate peak refinement method implemented in pDynamo (30)—but these gave the same overall picture as our NEB results, and so we do not report details of them here.

All QC calculations were carried out using the DFT methods within the ORCA program (version 2.9.1) (31). We tried a variety of DFT functionals, dispersion corrections, and basis sets, but unless otherwise stated, all QC calculations described here were performed with both the B3LYP hybrid (32, 33) and the BP86 GGA (34, 35) functionals, together with the Ahlrichs triple-zeta valence plus polarization (TZVP) basis set (36). The effect of water solvent was included in all DFT calculations via the COSMO implicit solvation model as implemented in ORCA (37).

Synthesis of cCys-Asn. The synthesis of protected cyclodipeptide Cys-Asn (cCys-Asn), the cyclization step, and the final deprotection were performed as described in the supplemental material.

Determination of the pK_a of the sulfhydryl group of cCys-Asn. The pK_a was determined by monitoring the absorbance at 240 nm of solutions of cCys-Asn adjusted at various pH values, as described in the supplemental material, in particular Fig. S6.

Acylation of the cCys-Asn dipeptide by β-lactams. The rates of acylation of cCys-Asn (0 to 1,000 μM) by β-lactams (100 μM) were determined in 100 mM sodium pyrophosphate (pH 8.2) at 20°C by monitoring variations in the absorbance at wavelengths specific for the rupture of the β-lactam ring of the carbapenems and of the cephems (λ = 298 nm for imipenem, λ = 486 nm for nitrocefin, λ = 299 nm for β-32, and λ = 265 nm for cefotaxime). The initial rates linearly increased with the concentration of the dipeptide. The apparent second-order rate constants for the acylation reaction were determined as described in the supplemental material.

Acylation of Ldt_{fm} by β-lactams. Quenching of the fluorescence of Trp residues of Ldt_{fm} was used to evaluate the apparent second-order rate constants for the acylation reaction (38). Fluorescence kinetics data were acquired with a stopped-flow apparatus coupled to a spectrofluorometer in 100 mM sodium phosphate (pH 6.0) at 20°C.

SUPPLEMENTAL MATERIAL

Supplemental material for this article may be found at https://doi.org/10.1128/AAC.02039-18.

SUPPLEMENTAL FILE 1, PDF file, 2.5 MB.

ACKNOWLEDGMENTS

We thank the Agence Nationale de la Recherche (grant ANR 2011 BSV5 024 01 to N.B., M.F., J.-E.H., J.-P.S., M.J.F., M.A. and C.M.B.) and the Fondation pour la Recherche Médicale (grant ECO20160736080 to Z.E.).

REFERENCES

1. Mainardi JL, Villet R, Bugg TD, Mayer C, Arthur M. 2008. Evolution of peptidoglycan biosynthesis under the selective pressure of antibiotics in Gram-positive bacteria. FEMS Microbiol Rev 32:386–408. https://doi.org/10.1111/j.1574-6976.2007.00097.x.
2. Hugonnet JE, Mengin-Lecreulx D, Monton A, den Blaauwen T, Carbonnelle E, Veckerle C, Brun YV, van Nieuwenhze M, Bouchier C, Tu K, Rice LB, Arthur M. 2016. Factors essential for L,D-transpeptidase-mediated peptidoglycan cross-linking and beta-lactam resistance in *Escherichia coli*. Elife 5:e19469. https://doi.org/10.7554/eLife.19469.
3. Mainardi JL, Hugonnet JE, Rusconi F, Fourgeaud M, Dubost L, Moumi AN, Delfosse V, Mayer C, Gutmann L, Rice LB, Arthur M. 2007. Unexpected inhibition of peptidoglycan LD-transpeptidase from *Enterococcus faecium* by the beta-lactam imipenem. J Biol Chem 282:30414–30422. https://doi.org/10.1074/jbc.M704286200.
4. Triboulet S, Dubée V, Lecoq L, Bougault C, Mainardi JL, Rice LB, Etheve-Quelquejeu M, Gutmann L, Marie A, Dubost L, Hugonnet JE, Simorre JP, Arthur M. 2013. Kinetic features of L,D-transpeptidase inactivation critical for beta-lactam antibacterial activity. PLoS One 8:e67831. https://doi.org/10.1371/journal.pone.0067831.
5. Lecoq L, Dubée V, Triboulet S, Bougault C, Hugonnet JE, Arthur M, Simorre JP. 2013. Structure of *Enterococcus faecium* L,D-transpeptidase acylated by ertapenem provides insight into the inactivation mechanism. ACS Chem Biol 8:1140–1146. https://doi.org/10.1021/cb4001603.

6. Dubée V, Arthur M, Fief H, Triboulet S, Mainardi J-L, Gutmann L, Sollogoub M, Rice L, Ethève-Quelquejeu M, Hugonnet J. 2012. Kinetic analysis of *Enterococcus faecium* L,D-transpeptidase inactivation by carbapenems. Antimicrob Agents Chemother 56:3409–3412. https://doi.org/10.1128/AAC.06398-11.
7. Edoo Z, Arthur M, Hugonnet JE. 2017. Reversible inactivation of a peptidoglycan transpeptidase by a beta-lactam antibiotic mediated by beta-lactam-ring recyclization in the enzyme active site. Sci Rep 7:9136. https://doi.org/10.1038/s41598-017-09341-8.
8. Field M. 2008. The pDynamo program for molecular simulations using hybrid quantum chemical and molecular mechanical potentials. J Chem Theory Comput 4:1151–1161. https://doi.org/10.1021/ct800092p.
9. Dewar MJS, Zoebisch EG, Healy EF, Stewart JJP. 1985. AM1: a new general purpose quantum mechanical molecular model. J Am Chem Soc 107:3902–3909. https://doi.org/10.1021/ja00299a024.
10. Massova I, Kollman PA. 1999. Quantum mechanical study of β-lactam reactivity: the effect of solvation on barriers of reaction and stability of transition states and reaction intermediates. J Phys Chem B 103:8628–8638. https://doi.org/10.1021/jp9923318.
11. Garcías R, Coll M, Donoso J, Muñoz F. 2006. Density functional theory study of the thiolysis reaction in penicillins. J Mol Struct Theochem 773:29–34. https://doi.org/10.1016/j.theochem.2006.07.001.
12. Melia C, Ferrer S, Moliner V, Tunon I, Bertran J. 2012. Computational study on hydrolysis of cefotaxime in gas phase and in aqueous solution. J Comput Chem 33:1948–1959. https://doi.org/10.1002/jcc.23030.
13. Meng F, Sun L, Wang H, Zhao X. 2008. Theoretical study of the hydrolysis of a model carbapenem: 1-aza-bicyclo[3,2,1]hept-2-ent-7-one. J Mol Struct Theochem 851:335–341. https://doi.org/10.1016/j.theochem.2007.11.031.
14. Galván IF, Field MJ. 2008. Improving the efficiency of the NEB reaction path finding algorithm. J Comput Chem 29:139–143. https://doi.org/10.1002/jcc.20780.
15. Aleksandrov A, Field MJ. 2012. A hybrid elastic band string algorithm for studies of enzymatic reactions. Phys Chem Chem Phys 14:12544–12553. https://doi.org/10.1039/c2cp40918f.
16. Pena-Gallego A, Cabaleiro-Lago EM, Fernandez-Ramos A, Hermida-Ramon JM, Martinez NE. 1999. An *ab initio* study of a model compound of penicillins. J Mol Struct Theochem 491:177–185. https://doi.org/10.1016/S0166-1280(99)00108-6.
17. Gad El-Karim IA, Aly AA, Amine MS, El-Alfy S. 2010. Quantum mechanical calculations of the cephalosporin nucleus. J Mol Graph Model 28:478–486. https://doi.org/10.1016/j.jmgm.2009.11.004.
18. Bhattacharjee N, Field MJ, Simorre JP, Arthur M, Bougault CM. 2016. Hybrid potential simulation of the acylation of *Enterococcus faecium* L,D-transpeptidase by carbapenems. J Phys Chem B 120:4767–4781. https://doi.org/10.1021/acs.jpcb.6b02836.
19. Ballinger P, Long F. 1960. Acid ionization constants of alcohols. II. Acidities of some substituted methanols and related compounds. J Am Chem Soc 82:795–798. https://doi.org/10.1021/ja01489a008.
20. Navarro PG, Blázquez IH, Osso BQ, Martínez de las Parras PJ, Puentedura MIM, García AAM. 2003. Penicillin degradation catalysed by Zn(II) ions in methanol. Int J Biol Macromol 33:159–166. https://doi.org/10.1016/S0141-8130(03)00081-3.
21. Radzicka A, Wolfenden R. 1995. A proficient enzyme. Science 267:90–93. https://doi.org/10.1126/science.7809611.
22. Frere JM, Joris B, Varetto L, Crine M. 1988. Structure-activity relationships in the beta-lactam family: an impossible dream. Biochem Pharmacol 37:125–132. https://doi.org/10.1016/0006-2952(88)90764-2.
23. Mainardi JL, Hugonnet JE, Gutmann L, Arthur M. 2011. Fighting resistant tuberculosis with old compounds: the carbapenem paradigm. Clin Microbiol Infect 17:1755–1756. https://doi.org/10.1111/j.1469-0691.2011.03699.x.
24. Diacon AH, van der Merwe L, Barnard M, von Groote-Bidlingmaier F, Lange C, García-Basteiro AL, Sevene E, Ballell L, Barros-Aguirre D. 2016. Beta-lactams against tuberculosis-new trick for an old dog? N Engl J Med 375:393–394. https://doi.org/10.1056/NEJMc1513236.
25. Dhar N, Dubée V, Ballell L, Cuinet G, Hugonnet J-L, Signorino-Gelo F, Barros D, Arthur M, McKinney J. 2015. Rapid cytolysis of *Mycobacterium tuberculosis* by faropenem, an orally bioavailable beta-lactam antibiotic. Antimicrob Agents Chemother 59:1308–1319. https://doi.org/10.1128/AAC.03461-14.
26. Hanwell MD, Curtis DE, Lonie DC, Vandermeersch T, Zurek E, Hutchison GR. 2012. Avogadro: an advanced semantic chemical editor, visualization, and analysis platform. J Cheminform 4:17. https://doi.org/10.1186/1758-2946-4-17.
27. Ratcliffe RW, Wildonger KJ, Di Michele L, Douglas AW, Hajdu R, Goegelman RT, Springer JP, Hirshfield J. 1989. Studies on the structures of imipenem, dehydropeptidase I-hydrolyzed imipenem, and related analogs. J Org Chem 54:653–660. https://doi.org/10.1021/jo00264a028.
28. Palmore GTR, Luo T-JM, McBride-Wieser MT, Picciotto EA, Mariuska Reynoso-Paz C. 1999. Engineering crystalline architecture with diketopiperazines: an investigation of the strength of hydrogen-bonded tapes based on the cyclic dipeptide of (S)-aspartic acid. Chem Mater 11:3315–3328. https://doi.org/10.1021/cm990400p.
29. Phillips JC, Braun R, Wang W, Gumbart J, Tajkhorshid E, Villa E, Chipot C, Skeel RD, Kale L, Schulten K. 2005. Scalable molecular dynamics with NAMD. J Comput Chem 26:1781–1802. https://doi.org/10.1002/jcc.20289.
30. Gisdon FJ, Culka M, Ullmann GM. 2016. PyCPR—a Python-based implementation of the conjugate peak refinement (CPR) algorithm for finding transition state structures. J Mol Model 22:242. https://doi.org/10.1007/s00894-016-3116-8.
31. Neese F. 2012. The ORCA program system. WIREs Comput Mol Sci 2:73–78. https://doi.org/10.1002/wcms.81.
32. Becke AD. 1988. Density-functional exchange-energy approximation with correct asymptotic behavior. Phys Rev A 38:3098–3100. https://doi.org/10.1103/PhysRevA.38.3098.
33. Lee C, Yang W, Parr RG. 1988. Development of the Colle-Salvetti correlation-energy formula into a functional of the electron density. Phys Rev B Condens Matter 37:785–789. https://doi.org/10.1103/PhysRevB.37.785.
34. Becke AD. 1993. Density functional thermochemistry. III. The role of exact exchange. J Chem Phys 98:5648–5652. https://doi.org/10.1063/1.464913.
35. Perdew JP. 1986. Density-functional approximation for the correlation energy of the inhomogeneous electron gas. Phys Rev B 33:8822–8824. https://doi.org/10.1103/PhysRevB.33.8822. (Erratum, 34:7406, 1986.) https://doi.org/10.1103/PhysRevB.34.7406.
36. Weigend F, Ahlrichs R. 2005. Balanced basis sets of split valence, triple zeta valence and quadruple zeta valence quality for H to Rn: design and assessment of accuracy. Phys Chem Chem Phys 7:3297–3305. https://doi.org/10.1039/b508541a.
37. Klamt A. 2011. The COSMO and COSMO-RS solvation models. WIREs Comput Mol Sci 1:699–709. https://doi.org/10.1002/wcms.56.
38. Dubée V, Triboulet S, Mainardi JL, Etheve-Quelquejeu M, Gutmann L, Marie A, Dubost L, Hugonnet JE, Arthur M. 2012. Inactivation of *Mycobacterium tuberculosis* L,D-transpeptidase LdtMt(1) by carbapenems and cephalosporins. Antimicrob Agents Chemother 56:4189–4195. https://doi.org/10.1128/AAC.00665-12.